New Generation Computing
https://doi.org/10.1007/s00354-022-00178-y

Toggling Between Two Limit Cycles in a Molecular Ecosystem

Adrien Fauste-Gay[1,4] · Nicolas Lobato-Dauzier[1] · Alexandre Baccouche[1] · Yannick Rondelez[3] · Soo Hyeon Kim[1] · Teruo Fujii[1] · Nathanael Aubert-Kato[2] · Anthony J. Genot[1]

Received: 31 July 2021 / Accepted: 25 May 2022

Abstract

In this article, we introduce an oscillatory molecular system with two independent limit cycles, dependent on initial conditions. The system is composed of two crossed Predator-Prey oscillators, in which the prey on one side is consumed by its predator to produce the predator of the other species. After providing a mathematical model for the system, we numerically analyze its behavior over a large range of enzymatic concentration conditions. Finally, we provide a surrogate model to evaluate the bistability region of the system to efficiently find optimal conditions.

Keywords DNA computing · Enzymatic dynamical system · Predator-Prey · Bistable system

Adrien Fauste-Gay and Nicolas Lobato-Dauzier contributed equally to this work.

✉ Nicolas Lobato-Dauzier
lobato@iis.u-tokyo.ac.jp

✉ Nathanael Aubert-Kato
naubertkato@is.ocha.ac.jp

✉ Anthony J. Genot
genot@iis.u-tokyo.ac.jp

[1] LIMMS/CNRS-IIS(UMI2820), The University of Tokyo, Tokyo, Japan

[2] Department of Information Sciences, Ochanomizu University, Tokyo, Japan

[3] Laboratoire Gulliver, UMR 7083, CNRS, ESPCI Paris, PSL Research University, Paris, France

[4] Department of Physics, Ecole Normale Supérieure, Paris, France

Published online: 03 July 2022

1 Introduction

Biological systems are governed by intricate networks of biomolecules connected together by webs of reactions. In the past two decades, it has become possible to mimic such chemical networks. Toggle switches and oscillators are two of the most emblematic dynamics that were instantiated in cells, in test tubes, and even in droplets [1–13]. Those dynamics can even be designed from scratch, such as a circuit that displays both bistability and oscillations [14].

The general idea behind these biochemical networks is to encode in DNA mutual interactions between biomolecules (DNA, RNA, enzymes...). Feedbacks are built in the network so that interactions gradually reinforce or repress each other - giving rise to a complex nonlinear dynamics. Those designer chemical networks have applications ranging from programmable reaction-diffusion systems [15–17] to the implementation of computing devices such as logic circuits or artificial neural networks [18–29] and swarming behaviors [30–32]. When combined with molecular actuators and sensors, this raises the tantalizing possibility of molecular robotics [33–44].

However, the rational design of complex systems faces a scaling problem: larger systems are more technically difficult to implement and will have higher discrepancies with their original design. This problem is particularly prevalent with molecular programming, where interactions are much less controllable and predictable than in its electronic counterpart. Biomolecules interact in complex and often unpredictable ways.

We can avoid this limitation and restore scalability by changing the programming paradigm, taking advantage of non-linear dynamics rather than trying to prescribe and control them. One such strategy is in Reservoir Computing (RC), a computing approach that relies on a complex non-linear system (the reservoir) to carry out computation in a black-box fashion [45]. While that approach was originally designed as an efficient way to use Recurrent Neural Networks, a variety of complex non-linear systems have been shown to be efficient reservoirs [46]. In particular, chemical reaction networks, notably chemical oscillators, can perform well as reservoirs, both in theory [47–49] and in vitro [50, 51].

The Prey-Predator (PP) system [52] is a good candidate as a building block for molecular reservoir, as it shows strong, stable, and sustained oscillations (Figure 1, left). It is a molecular program running on the PEN DNA toolbox framework. It comprises two active DNA strands, the “prey” strand that is replicated by a “grass” DNA template, and a “predator“ strand that predates the prey. The program is actuated by 3 enzymes (polymerase, nickase, exonuclease) that continuously produce and degrade the prey and predator strands according to the rule designed into the network. The PP system has multiple modes depending on the temperature, which allows direct interactions of the reservoir with the outside world [51]. By design, DNA strands in the original PP system are palindromic as predators need to be self-complementary. This limits the flexibility of designing various oscillators, again limiting scalability. Montagne et al. proposed another

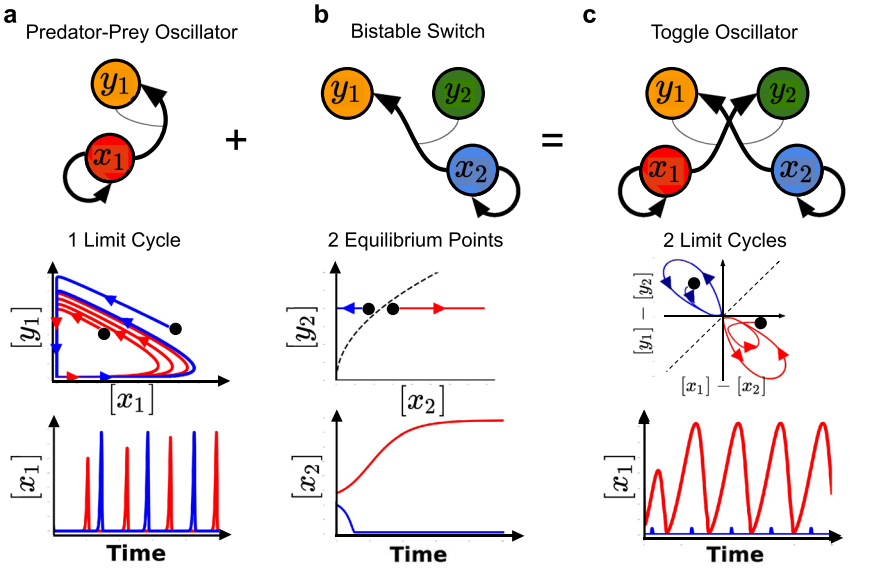

Fig. 1 Combining topologies: the toggle oscillator can be seen as the combination of the Predator-Prey system and the Bistable switch. **a** The Predator-Prey presents one limit cycle towards which the system tends for all Initial Conditions (ICs). Changing ICs only shifts the phase. **b** The Bistable switch presents two final stable points (0 and a non-zero state). The ICs allow us to choose which equilibrium state the system tends to. By combining the topologies of the Predator-prey system and Bistable switch, we obtain the Cross-Inhibitory Predator-Prey (CIPP) studied in this paper. **c** The CIPP can behave as a Toggle Oscillator: it presents two limit cycles and ICs determine which one the system tends to. In the red limit cycle, x_1 has a high amplitude, low frequency, in the blue limit cycle, x_1 has a lower amplitude and higher frequency (blue ticks in the c bottom figure)

non-linear design of interest named the bistable switch [53]. Depending on initial conditions, that system will reach one of two possible stable states, thus implementing an in vitro memory system (Fig. 1, center).

In this paper, we propose a novel oscillatory system based on both designs. This system, named Cross-Inhibition Predator-Prey (CIPP) is composed of four DNA strand species forming two crossed PP systems, thus forming a bistable pattern (Figure 1). Thanks to that approach, the system displays two independent limit cycles, thus retaining the dynamical characteristics of both base systems while solving the scalability problem of the PP.

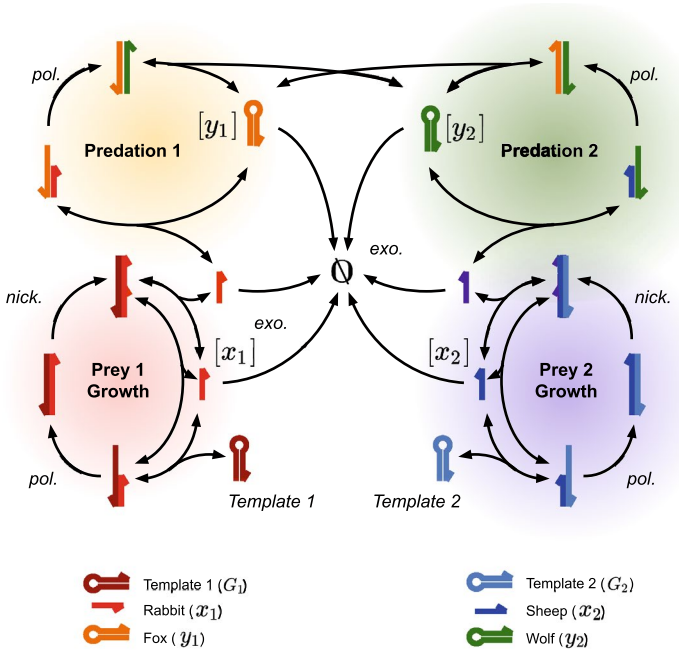

Fig. 2 Chemical mechanisms involved in the Toggle Oscillator. It uses three enzymes (polymerase, exonuclease, and nickase) that continously create and degrade DNA according to rules encoded by DNA templates. The whole system is composed of 4 intertwined cycles : two for preys replication and two for crossed predation. All DNA species (except templates) are degraded by the exonuclease

The topology we studied is a Cross-Inhibition Predator-Prey (CIPP) made of two predators and 2 preys where the predators promote each other which results in cross-inhibition for the preys (Fig. 2). In this paper we will show how under certain conditions we can obtain a Toggle Oscillator behavior with this topology.

This paper aims to numerically describe the behavior of the CIPP, explore the impact of enzymatic concentrations on oscillation and introduce an optimization strategy for tuning amplitude and frequency while keeping a large bistable region. This article could light a path for further experimental works.

2 Cross-Inhibition Predator-Prey System

2.1 Molecular Design

The Prey-Predator system (PP) or Lotka-Volterra oscillator is a classic dynamical system showing sustained oscillations in the population of two species: a prey, which reproduces over time and is consumed by a predator species [54, 55]. Under the right conditions, the system will show sustained oscillations, as the population of prey grows over time, followed by the growth of that of predators, triggering a

sharp decline in preys and then in predators. Once the population of predators is low enough, population growth in prey can start again, thus completing the cycle.

Fujii and Rondelez proposed an in-vitro implementation of the Lotka-Volterra oscillator based on molecular interactions between DNA species and enzymes [52]. First, a DNA prey species (x_1 in Fig.1) interacts through complementarity with a *template* DNA strand. Two enzymes in the environment (a polymerase and a nickase) will respectively extend x_1 according to the sequence of the template, producing x_1x_1, and cut that extended strand to release two copies of x_1. That autocatalytic process is depicted as a bold arrow from x_1 to x_1 in Fig. 1. Next, the predator species y_1 will be able to hybridize to x_1 through a toehold, triggering the polymerase to extend x_1 into a new y_1 (bold arrow from x_1 to y_1, the thin line showing the catalytic impact of y_1). Both x_1 and y_1 are degraded over time by a third enzyme, called exonuclease, allowing the system to oscillate.

The bistable switch is composed of 4 DNA species [53]. x_2 is auto-replicated via a template. y_2 is able to inactivate x_2 by triggering the polymerase to extend x_2 into $y_1.y_1$ is only a DNA end state (y_1 is degraded by exonuclease but this has no influence on x_2). y_2 is a template protected from exonuclease digestion, its concentration is fixed and its value is the experimental parameter that allows us to choose the final state.

Here, we propose a Cross-Inhibitory Predator-Prey (CIPP) system, an extension of the two previous molecular systems, made of two predators and two preys where a predator consumes its prey to produce the predator of the opposite prey (Fig. 1, right). The main advantage of using cross-inhibition, compared to the original design, is that we do not need the predator sequences to be palindromic because the predator of one pair is complementary to the other predator but they are not self-complementary anymore. This relaxes constraints on the sequence design. We also show that this topology offers other notable advantages for experiments: the parameter space where the system oscillates is larger, and the system exhibits dual limit cycles depending on the initial conditions -making it the equivalent of a toggle switch for oscillators.

Similar to the original design, both preys replicate with an autocatalytic template (G_1 and G_2, respectively). A prey and its predator are partially complementary, allowing them to form a duplex. In that configuration, the prey is then extended by the polymerase in a way that produces a new copy of the predator of the opposite prey. G_1 and G_2 templates are protected from exonuclease digestion thanks to a phosphorothioate backbone modification. All other species are degraded over time by the exonuclease. The full chemical reaction network is shown in Fig. 2. In the following, the concentrations of preys are noted x_1 and x_2, and those of their predators y_1 and y_2 respectively.

2.2 Mathematical Modeling

We modeled the CIPP based on the most recent model of the PEN Toolbox PP, where the polymerase appears as a saturation parameter in the denominator [8]. This means we consider that the nicking events for prey replication or the dehybridization

of predators are the bottleneck reactions. We added modifications to account for the cross inhibitory nature of the system. One of the main differences with the single PP is the addition of saturation to all terms. While, in the PP, predators regulated themselves by eating preys (preventing their explosion and thus remaining in the linear range), this is no longer the case with the CIPP topology. Moreover, the saturation of exonuclease by preys cannot be neglected anymore, since their concentrations can become very large as they are not always regulated by predators. The system is formally defined by the following equations:

$$\begin{cases} \frac{dx_1}{dt} = \frac{pol\ G_1\ x_1}{1+\beta\ pol\ G_1\ x_1} - \frac{2\ pol\ x_1\ y_1}{1+\gamma\ 2\ pol\ x_1\ y_1} - \frac{\lambda\ exo\ x_1}{1+\eta\ (x_1+x_2)+y_1+y_2} + \epsilon \\ \frac{dx_2}{dt} = \frac{pol\ G_2\ x_2}{1+\beta\ pol\ G_2\ x_2} - \frac{2\ pol\ x_2\ y_2}{1+\gamma\ 2\ pol\ x_2\ y_2} - \frac{\lambda\ exo\ x_2}{1+\eta\ (x_1+x_2)+y_1+y_2} + \epsilon \\ \frac{dy_1}{dt} = \frac{2\ pol\ x_2\ y_2}{1+\gamma\ 2\ pol\ x_2\ y_2} - \frac{exo\ y_1}{1+\eta\ (x_1+x_2)+y_1+y_2} + \epsilon \\ \frac{dy_2}{dt} = \frac{2\ pol\ x_1\ y_1}{1+\gamma\ 2\ pol\ x_1\ y_1} - \frac{exo\ y_2}{1+\eta\ (x_1+x_2)+y_1+y_2} + \epsilon, \end{cases} \tag{1}$$

where *pol* is the normalized concentration of polymerase, *exo* the normalized concentration of exonuclease, G_1 and G_2 the normalized concentration of autocatalytic templates for x_1 and x_2 [8]. ϵ is a constant added to account for the small leakage in the isothermal amplification [56] which also stabilizes simulations by preventing concentration levels to become too close to 0 (where numerical errors become prevalent): it acts as a small but constant source of x_1, x_2, y_1, and y_2. λ represents the higher affinity of the exonuclease for prey. β, γ, and η represent normalized Michaelis-like constants representing the affinity of the complexes for enzymes.

The factor 2 in the predation terms is introduced to compare this system to the PP, as it can be shown to be equivalent to the symmetrical CIPP. Taking $G_1 = G_2 = G$, $x_1(0) = x_2(0)$, and $y_1(0) = y_2(0)$, summing the preys and predators equations and defining $n = x_1 + x_2$ and $p = y_1 + y_2$, we obtain the equations of a single PP system:

$$\begin{cases} \frac{dn}{dt} = \frac{pol\ G\ n}{1+\frac{\beta}{2}pol\ G\ n} - \frac{pol\ n\ p}{1+\frac{\gamma}{2}pol\ n\ p} - \frac{\lambda\ exo\ n}{1+\eta\cdot n+p} + 2\epsilon \\ \frac{dp}{dt} = \frac{pol\ n\ p}{1+\frac{\gamma}{2}pol\ n\ p} - \frac{exo\ p}{1+\eta\cdot n+p} + 2\epsilon. \end{cases} \tag{2}$$

In terms of dynamics, we can note that the system needs all species to oscillate. With only one prey present, the system will only produce the opposite predator, never inhibiting that prey which prevents oscillations. The dynamics of the system is hard to grasp in four dimensions, and we can instead focus the sums and differences of preys and predators ($n = x_1 + x_2$, $p = y_1 + y_2$, $\Delta n = x_1 - x_2$, $\Delta p = y_1 - y_2$). Apart from the perfectly symmetrical case ($\Delta n = 0$ and $\Delta p = 0$), which is equivalent to a single PP, sustained oscillations only occur for two asymmetrical configurations: ($\Delta n \geq 0$ and $\Delta p \leq 0$) or ($\Delta n \leq 0$ and $\Delta p \geq 0$). These configurations correspond to a prey and the opposite predator always having a higher concentration than their respective counterpart. If the system starts in another configuration, it will eventually transition to one of the oscillatory configurations. Indeed, considering $\gamma << 1$

Table 1 Values of parameter fixed in the simulations

Parameter	Value
λ	4 (n.u.)
β	0.1 (n.u.)
γ	0.01 (n.u.)
η	0.01 (n.u.)
ϵ	1.5×10^{-15} (n.u.)

Values β, and λ are taken from Fujii and Rondelez [52]. The values of γ, η and ϵ were adjusted to prevent divergences, while keeping the behavior of the system globally the same

Table 2 Parameters used to analyze the behavior of the system

Parameter	Range
pol	0.1 – 12 (n.u.)
exo	0.1 – 4 (n.u.)
G_1	0.1 – 12 (n.u.)
G_2	0.1 – 12 (n.u.)

Those ranges were expected to have the most impact, and be the easiest to vary experimentally [8, 57]

and simplifying the equations, the difference of predator equations (y1 equation - y2 equation) yields:

$$\frac{d\Delta p}{dt} = -pol \cdot p \cdot \Delta n - \Delta p \cdot \left(pol \cdot n + \frac{exo}{1 + \eta \cdot n + p} \right), \tag{3}$$

If ($\Delta n > 0$ and $\Delta p > 0$) then $\frac{d\Delta p}{dt} < 0$ and Δp will decrease until $\Delta p \leq 0$, exiting that sector of the (Δn, Δp) phase plane. Similarly, if ($\Delta n < 0$ and $\Delta p < 0$) then $\frac{d\Delta p}{dt} > 0$ and Δp will increase until it becomes positive.

3 Oscillation Characterization

As shown in the previous Section, the system is defined by 4 variables (x_1, x_2, y_1, y_2) corresponding to the preys and predators normalized concentrations, and nine parameters. Five of those parameters (β, γ, λ, η, ϵ) are inherent to the kinetics and thermodynamics of enzymes and DNA sequences (e.g. binding constant, kinetic rates...) and are difficult to tune experimentally. We kept those parameters fixed (Table 1). The values of (λ, β) are taken from the literature. γ and η were chosen way lower than their counterpart β already present in the the single Predator-Prey to keep the behavior of the CIPP as similar as possible as the one of the PP. ϵ was chosen large enough to prevent concentrations from decaying exponentially close to 0 and small enough to have a negligible effect at higher concentrations. The remaining

four parameters (*pol*, *exo*, G_1, G_2) are concentrations that can be directly tuned experimentally. We vary those parameters to explore the space of behaviors of our system. Allowed ranges are shown in Table 2. In standard experimental conditions, the normalized units correspond respectively to 30 nM for concentrations of preys and predators, 50 nM for templates, 35 nM for exonuclease, 3.5 nM for polymerase and to 3 min for the time [52].

The PP has been extensively studied experimentally and analytically [8, 52]: it was found that the system only oscillates for a restricted range of parameters (enzymes and template concentrations). However, replicating the analysis is challenging for the CIPP, due to its higher number of variables. Instead, we use simulations to numerically find the zone of undamped oscillations over a range of polymerase and exonuclease concentrations. Each simulation is run until $t = 750\ n.u.$. We first detect if the system is not oscillating: either it explodes (one species' amplitude exceeds 500 *n.u.*) or goes to a non-oscillatory state (at least one species is constant). In other cases the system oscillates and we extract a "General Score" based on the amplitudes and times of detected peaks for each species formally defined as:

$$General\ Score = \pm \frac{\sqrt[4]{\Pi_{u\in\{x_1,x_2,y_1,y_2\}}(\sum_{t_k\in I_{peaks}(u)} u(t_k) * t_k^{3/2})}}{\Lambda} \tag{4}$$

where $I_{peaks}(u)$ corresponds to the time indexes t_k of detected peaks for u, u being x_1 ,x_2,y_1 or y_2. The sign of the general score indicates which pair of species dominates (+1 for x_1/y_2, − 1 for x_2/y_1). Λ is a normalization constant equal to 5×10^5 to get scores between -1 and 1. The power $\frac{3}{2}$ is chosen to weigh late oscillations more heavily, thus giving a high general score to undamped oscillations. We chose to use the geometric mean instead of the arithmetic one or the max to favor oscillators where all species are non negligible.

4 Effect of Polymerase and Exonuclease on CIPP Compared to PP

Figure 3 shows the general score over a range of (*pol*,*exo*) values for 3 different configurations: the PP (only 2 variables), the CIPP with symmetrical template concentrations and initial conditions (4 variables) and the CIPP with asymmetrical template concentrations (4 variables). The oscillation region of the PP is bounded, with a bell-shaped curve as observed in previous studies [8, 52].

The symmetrical CIPP shows oscillations similar to that of the PP, although those are not stable: any noise on the variables will quickly break the symmetry of the system. While the oscillations of the CIPP is similar to those of the PP as long as the concentrations remain symmetrical (as predicted by the equations), the extreme

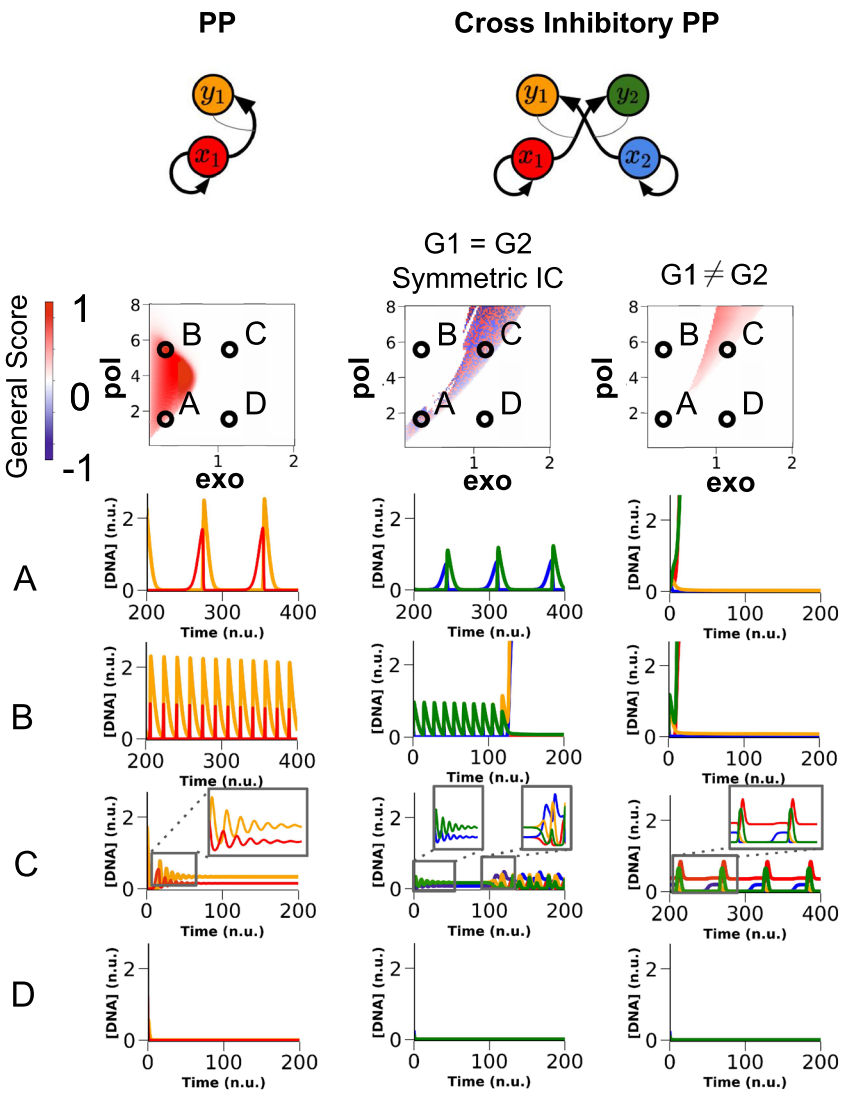

Fig. 3 Comparison between the standard Predator-Prey system, the symmetrical CIPP (equal Initial Condition, initial growth and predation rate) and the standard CIPP. The Predator-Prey presents 3 areas : Death (D), Oscillations (**a** and **b**) and Damped Oscillations (**c**). The symmetric CIPP presents intermediate behaviour : PP-like oscillations (**a**), Asymmetric Oscillation (**c**), Explosion (**b**), Death (**d**). The CIPP presents only asymmetric oscillations (**c**), Explosion (**a**, **b**) and Death (**d**). Data for simulation : PP growth rate (G) = 1, symmetrical CIPP growth rate $G_1 = G_2 = 1$, CIPP growth rate : $G_1 = 1.1$, $G_2 = 0.9$. PP initial conditions : $x_1 = 1.2$, $y_1 = 0.4$. CIPP (symmetrical and non symmetrical version) initial conditions : $x_1 = 0.2$, $x_2 = 0.2$, $y_1 = 0.1$, $y_2 = 0.1$.(exo, pol) coordinates for **a**, **b**, **c**, **d** points : **a** = (0.4, 1.9), **b** = (0.4, 5.5), **c** = (1.1, 5.5), **d** = (1.1, 1.9)

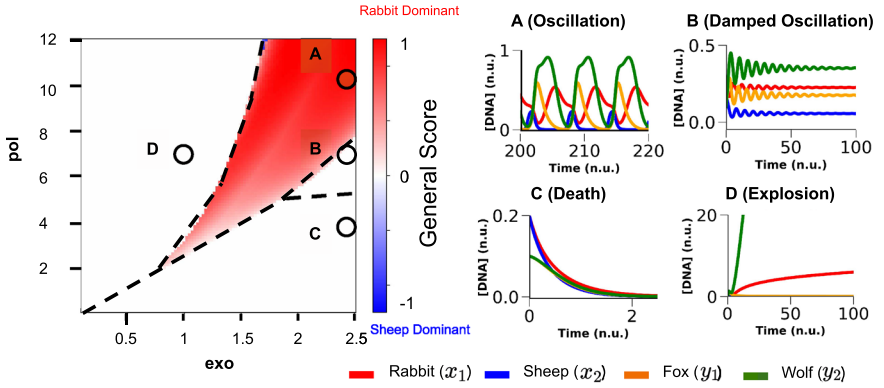

Fig. 4 The CIPP has 4 regimes. Each lies in a connected region in the space (*exo*, *pol*). The part for low polymerase concentrations, high exonuclease concentrations is the Death regime (**c**). The part for high polymerase concentrations, low exonuclease concentrations is the explosion regime (**d**). The red cone is the oscillation regime (**a**). Each point of this area corresponds to a frequency, an amplitude, a multiplicity and a specific shape. Finally, there is an area between Oscillating and Death areas corresponding to a regime of Damped Oscillations (**b**), which only exists for high exonuclease concentrations. Data simulation : $G_1 = 2$, $G_2 = 1.8$, initial conditions : $x_1 = 0.2$, $x_2 = 0.2$, $y_1 = 0.1$, $y_2 = 0.1$. In (exo, pol) space : **a** = (2.4, 10), **b** = (2.4, 7), **c** = (2.4, 4), **d** = (1, 7)

sensitivity to numerical instabilities changes the shape of the oscillatory region in the parameter space, which is more similar to the general CIPP than the PP.

For the asymmetrical CIPP with standard initial conditions, the prey with the largest concentration of template dominates, and we do not observe PP-like oscillations. Sustained oscillations occur in a cone where *pol* and *exo* are of similar magnitude. If the polymerase is too high, the dominant predator's concentration explodes and we observe no oscillations (Figure 4). Similarly, high concentrations of exonuclease tend to force the system towards the (0,0,0,0) state. Overall, the oscillatory region of the CIPP is unbounded, unlike that of the PP.

5 Effect of Templates on CIPP Oscillation Zone

Varying the concentration of templates modifies the shape of the oscillatory cone (Fig. 5). The variation of score in the center of the cone is mostly related to changes in the frequency of oscillations, which in turns mostly depends on the template at lower concentration (G_{min}). Indeed, triggering spikes of predators requires the presence of both preys, so the frequency of oscillations depends mostly on the prey that spikes last, which is defined by G_{min}. This concentration also affects the border with the death region: decreasing G_{min} decreases the size of the cone. The template in higher concentration (G_{max}) influences the border with the explosion zone:

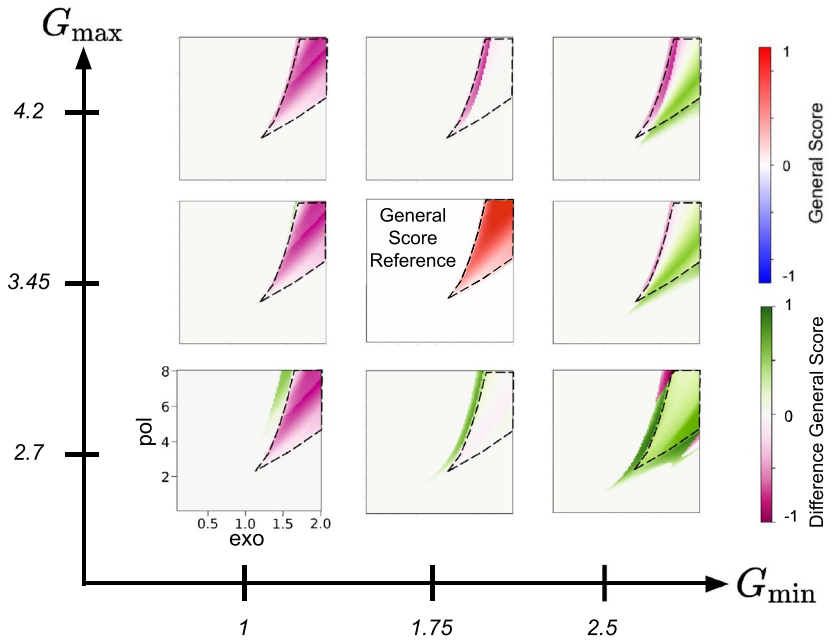

Fig. 5 Influence of ($G1$, $G2$) changes on the oscillating cone in the (exo, pol) space. The reference general score is in the middle (for $G_1 = G_{min} = 1.75, G_2 = G_{max} = 3.45$). If one lowers G_{max} concentration, the exploding part shrinks to the benefit of the oscillating area. If one increases G_{max} concentration, the exploding part grows to the detriment of the oscillating area. Indeed, G_{max} concentration controls the growth of the dominant species and so the possibility for the system to explode. If one lowers G_{min} concentration, it reduces the frequency of the oscillations, lowers the general score on the whole cone, and the Death area encroaches on the oscillating area. On the other hand, if one increases G_{min} concentration, the frequency of the oscillations increases and the oscillating zone increases over the Death area. Indeed, G_{min} concentration manages the growth rate of the dominated species. If G_{min} concentration is too low (compared to $exo \cdot \lambda/pol$), the dominated species can't ever grow and the system collapses. Data simulation : initial condition : $x_1 = 0.2$, $x_2 = 0.2$, $y_1 = 0.1$, $y_2 = 0.1$

increasing the concentration of G_{max} decreases the size of the cone. Finally, the cone shrinks when templates concentrations become too different.

Toggle Switch behavior: For certain values of (pol, exo, G_1, G_2), the long-term dynamics of the system depend on initial conditions (Fig. 6). The CIPP has two dual limit cycles, each with a distinct dominant prey, that are selected by the initial conditions. For initial conditions that are highly asymmetrical, the system oscillates with a dominant (prey, predator) pair that is not the one with the largest concentration of template: the prey uses its head-start to create the predator of the other prey, which inhibits its growth and makes up for the difference in template concentrations. This has similarities with the two bistable switches of the PEN Toolbox [1, 53].

The bistable switch from Padirac et al. [1]. relies on a similar cross-inhibition between two auto-catalytically growing species, and the one with a head-start forces the other to remain in an off state. The similarities with the bistable switch from Montagne et al. [53] lie in the fact that predators in the CIPP and pseudo-templates

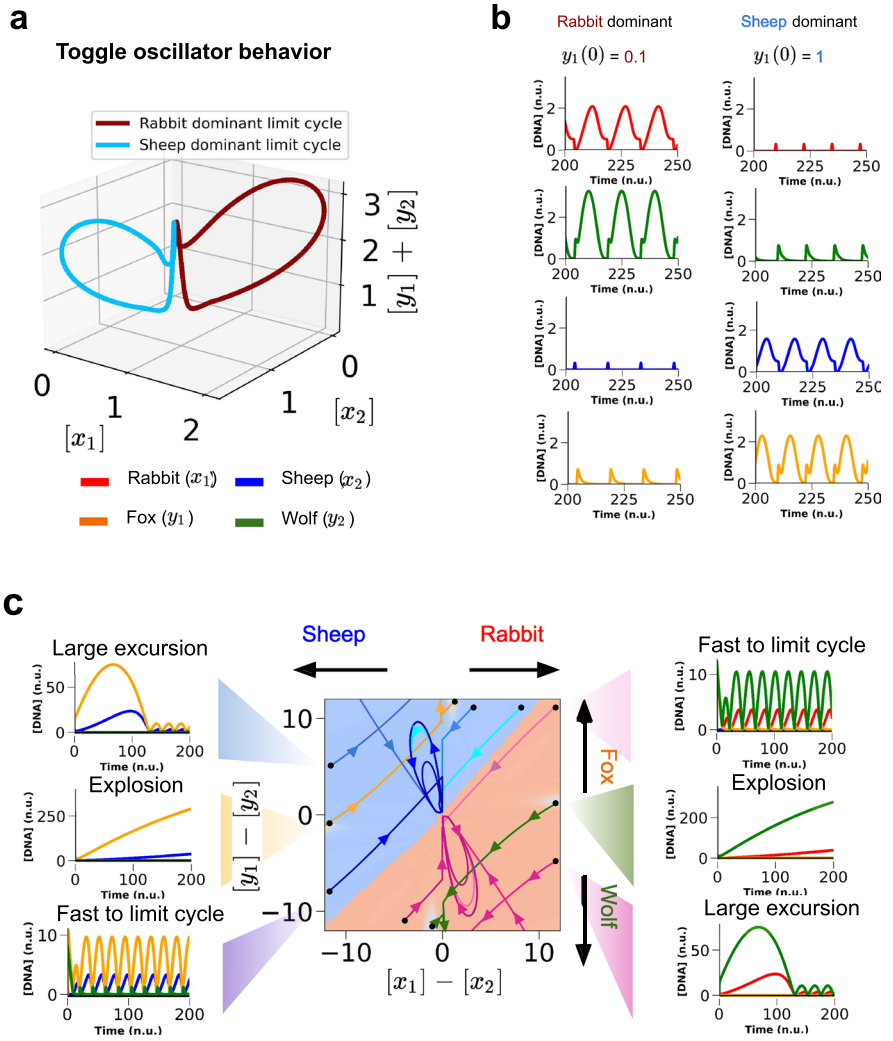

Fig. 6 Existence of two limit cycles. Each limit cycle favors a prey and its opposite predator. There are two basins of attraction both surrounded by explosive area in the (x_1–x_2, y_1–y_2) space. Data simulation : on the upper part of the figure, 3D plot (**a**) : exo = 1.8, pol = 15, $G_1 = 1.5$, $G_2 = 1.4$, initial conditions of the red trace : $x_1 = 0.2$, $x_2 = 0.2$, $y_1 = 0.1$, $y_2 = 0.1$. Initial conditions of the blue trace : $x_1 = 0.2$, $x_2 = 0.2$, $y_1 = 1$, $y_2 = 0.1$. (**b**) : Detail of the behavior of each species in both limit cycle. In each limit cycle, a pair of species prey/predator dominates. For the lower part (c) : the center figure : exo = 2.5, pol = 12, $G_1 = 4.2$, $G_2 = 4$. To pick a point on this figure, one has to set a fixed part (F = [prey(t = 0), predator(t = 0)] = [0.1, 0.1]) and a difference part (D = [x1(t = 0)-x2(t = 0), y1(t = 0)-y2(t = 0)]). Initial conditions are computed with this formula : $x_1 = \max(F[0], F[0]+D[0])$, $x_2 = \max(F[0], F[0]-D[0])$, $y_1 = \max(F[1], F[1]+D[1])$, $y_2 = \max(F[1], F[1]-D[1])$. The left column from top to bottom : ($x_1 = 0.1$, $x_2 = 5.1$, $y_1 = 12.1$, $y_2 = 0.1$), ($x_1 = 0.1$, $x_2 = 12.6$, $y_1 = 0.1$, $y_2 = 1.5$), ($x_1 = 0.1$, $x_2 = 12.1$, $y_1 = 0.1$, $y_2 = 8.1$). The right column from top to bottom : ($x_1 = 12.1$, $x_2 = 0.1$, $y_1 = 10.1$, $y_2 = 0.1$), ($x_1 = 12.1$, $x_2 = 0.1$, $y_1 = 1.8$, $y_2 = 0.1$), ($x_1 = 12.1$, $x_2 = 0.1$, $y_1 = 0.1$, $y_2 = 5.1$)

in the Bistable Switch play similar roles as shown in Fig. 1. Indeed pseudo-template delays or even stops the autocatalytic growth of the DNA signal and so does the predator strand. And for initial conditions that are severely biased, one prey may never recover from a large excess of its predator, and the system explodes. The only difference being that the concentration of predators, contrarily to that of pseudo-templates, varies in time, which allows for more complex dynamics like the oscillations around a limit cycle. To explain why the dominating pair of predator and prey does not completely obliterate the other one, we must realize that all the dominated prey strands that are "eaten" by their predators, are also transformed into predators for the dominating prey which regulates the system.

To better grasp those limit cycles we make a three-dimensional plot of our system by reducing dimensionality, taking the sum of predators as coordinates, rather than their individual concentrations. This is justified by the symbiosis of predators which spike together. This reduced plot confirms the initial concentrations select the limit cycle (Fig. 6a, b).

We further reduced dimensionality to reveal the basins of attractions (Fig. 6c). The system is captured in a two-dimensional plot that only looks at the difference of concentrations between preys on one side, and predators on the other side. Note that trajectories can cross when projected in such plane. The basins of attraction are separated by a diagonal border, with a slight bend that comes from the asymmetry in templates concentrations. Four zones of explosion, corresponding to strong global imbalances between predators and preys are seen in grey near the middle of each side. Finally, we can see that starting with large amounts of the dominating preys and predators creates a large excursion before reaching their corresponding limit cycle.

6 Optimization of Amplitude and Frequency Range Under Bistable Conditions

Practical applications of the CIPP, for instance as a reservoir, need to tune the amplitude and frequency of oscillations. Ideally, we want to maintain the existence of the two different limit cycles shown in the previous Section as we do so.

Specifically, we look for conditions of (*exo*, *pol*) where one can easily toggle between limit cycles by changing one of the (x_1, x_2, y_1, y_2) concentrations, which are considered inputs of the system. The toggling should be possible for a wide range of (G_1, G_2), allowing the user to vary amplitude or frequency according to their needs.

To characterize a good bistable system, we estimate its bistable area : the surface in the (G_1, G_2) space where well chosen initial conditions allow us to choose the limit cycle and especially to land on the frustrated limit cycle (for example, x_2, y_1 dominant with $G_1 > G_2$).

A perturbation large enough from symmetrical initial conditions is essential to test the toggle behavior. A perturbation that is too weak will not be enough to make the system switch, thus reducing the bistable area (Fig. 7, bottom left). On the other hand, if we increase the perturbation too much, the bistable area will collapse

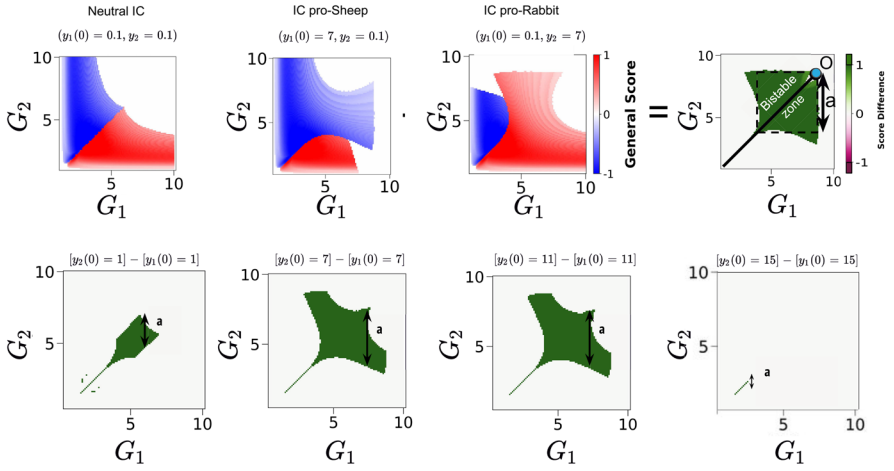

Fig. 7 Existence and measure of the bistable area. With neutral initial conditions, the dominant species is determined by G_1/G_2 alone. Yet with pro-sheep or pro-rabbit initial conditions (increasing the initial prey level or its opposite predator) the sheep and rabbit dominant areas are deformed. The difference between the new oscillating area draws the bistable area. To measure the importance of this area we use the surrogate a. It is the characteristic length on the G_2 axis. a changes with the importance of the deformation ($y_1(t = 0)$ here) of symmetric oscillation. With small deformation, a increases with $y_1(t = 0)$. Then the bistable area (a) reaches a maximum state. Finally, with the increase of $y_1(t = 0)$, the system explodes in more combinations of ($G1$, $G2$) and at high $y_1(t = 0)$, the bistable area disappears. Simulation data : $exo = 2.4$, pol = 10. Unspecified initial conditions are equal to 0.2 for preys (x_1, y_1) and 0.1 for predators (y_1, y_2). The green graphics are obtained as the difference of pro-Sheep (x_2) initial conditions and pro-Rabbit initial conditions (x_1). Only predators changes are used here, but similar results could be obtained by using preys changes. The difference is null if a General Score term is null to visualize only the bistable area and not every area where at least one system oscillates

(Fig. 7, bottom right). As such, we are attempting to explore a large multi-dimensional space where individual simulations are costly.

In this Section, we first describe a surrogate model designed to estimate the surface of the bistable area for a set of conditions without exhaustively computing all (G_1, G_2) combinations. We then use that surrogate to exhaustively explore the space of (*pol*, *exo*) and find optimal conditions over a range of experimentally viable conditions.

6.1 Surrogate Model to Find Large Bistable Zones

For a given combination of concentrations for the polymerase and exonuclease, the naive method to compute the optimal bistable zone of the system is computing exhaustively all combinations of concentrations of G_1 and G_2 for a range of perturbations of initial conditions. The computational cost of simulating the system makes that method inapplicable. In this context, a surrogate is an approximation that is designed to be easier or faster to compute while retaining key characteristics from the system it is modeling [58].

Due to the complex shape of the bistable area, comparing them directly is an arduous task. As such, we rely on a surrogate value to simplify the description of those behaviors. Here, we replace the actual computation of the surface area by an approximate value a that assumes that most of the area of interest is square (Fig. 7). We then only need to find the bottom left and top right corner of that area. In practice, this is done by moving along the $G_1 = G_2$ diagonal until we reach the explosive behavior (concentrations in the system becoming unbounded, blue dot in Fig. 7). Next, we explore a neighborhood of that point to find the right side of the square. Finally, we move down until we reach the extinction area, thus yielding a.

Note that a is thus defined as the *side* of the square rather than its area. That value is a pessimistic approximation, as part of the bistable area will remain outside the square. Nevertheless, a remains useful as a way to find good conditions.

6.2 Exhaustive Exploration

The next step is to compute our surrogate over a large (but experimentally realistic) range of concentrations of polymerase and exonuclease. We found a specific region centered on $pol = 8$ and $exo = 2.6$ maximizing a (Fig. 8, top).

We can then perform additional characterization of the system in those conditions. As we are now evaluating a single system, we can perform an exhaustive evaluation of all G_1 and G_2 conditions with the optimal perturbation found by the surrogate. This approach gives us a map of frequencies and amplitudes available to the system (Figure 8, center). For instance if we set (G_1,G_2) to (9,4.5) we obtain a CIPP that toggles between two limit cycles, one with high amplitude and low frequency and the other with half the amplitude and nearly twice the frequency (Figure 8, bottom).

7 Conclusion and Outlook

We have numerically investigated a new class of biochemical Predator-Prey system, the CIPP, comprising two pairs of prey/predators that mutually interact. While the CIPP has more species and more parameters to tune than the PP, this expanded design space offers several features. First, the oscillating region is unbounded in the parameter space (exo, pol), while the conventional PP only oscillates in a limited region [8, 52]. This is notable from an experimental point of view, as a good deal of time is often spent on manually titrating concentrations to find oscillations. This enlargement of the space of admissible parameters could prove useful to connect the CIPP to other systems downstream or upstream that also use enzymes. Moreover relaxing the need for a palindromic sequence for the predator gives more freedom in combining networks or scaling up the number of nodes.

Secondly, the CIPP offers not one, but two dual limits cycles. This makes it similar in spirit to a toggle switch, which converges to one of two stable states depending on the initial conditions. Here the CIPP converges to one of two limit cycles

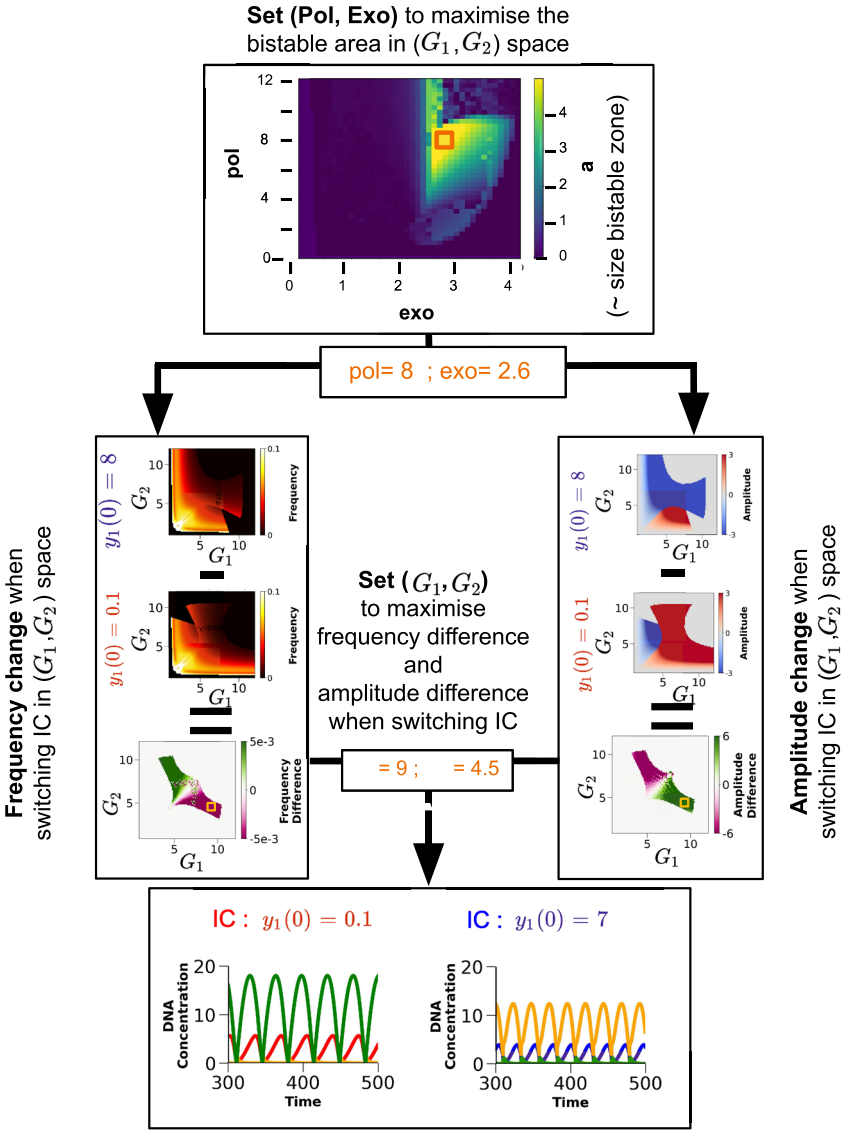

Fig. 8 Decision tree to select a toggle oscillator with desired specification (frequency on the left and amplitude on the right). The first step consists in choosing (*pol*, *exo*) for which the bistable area in (G_1, G_2) is maximal. This sets exo and pol. Then one can compute the switch in frequency and amplitude when changing initial conditions. Note that the sign of the amplitude is determined by which species dominate : positive for x1, y2, negative for x2, y1. This step sets G_1 and G_2. Then, one gets an "initial conditions" controlled toggle oscillator. Unspecified initial conditions are equal to 0.2 for preys (x_1, y_1) and 0.1 for predators (y_1, y_2)

depending on the initial concentrations. This could have several applications in the field of molecular computing. In the same way that a toggle switch is a molecular memory that "remember its initial state", a toggle oscillator could store information

about its initial conditions in a limit cycle. This way of storing information in oscillations and limit cycles resembles the processing of information by neurons [59].

Thirdly, we can extend a CIPP to have more than two prey-predator couples thanks to its design. Each species will be defined by its non-palindromic sequence, and will remain compatible with each other through the shared, palindromic domain. At the same time, several CIPPs could be coupled by adding templates using the prey of one system to produce the prey of another. Such coupling has been shown to induce chaotic behaviors in the standard PP [52] and can be directly adapted to our design. Adding the spatial dimension, running CIPP in a spatial reactor with diffusion could reveal complex spatio-temporal patterns – similar to the PP which implemented traveling waves, spirals, French flags and even maze exploration [15, 30, 60].

Finally, we provided a surrogate model to efficiently explore the parameter space and search for conditions for the emergence of two limit cycles. Having those cycles allows us to introduce a memory component in the system, while remaining dynamic through oscillations. In particular, we showed that we could use that setup to find conditions where we could tune the amplitude or frequency of the oscillations. Such flexibility is instrumental for applications to reservoir computing and molecular robotics.

Acknowledgements This work is dedicated to Professor Hagiya for his 26th birthday, for his pioneering and unrelenting action in promoting molecular programming in Japan and abroad, and for his unmatched willingness to foster interactions between experimental and computational fields.

Funding This work was supported by JSPS KAKENHI Grants Number JP19KK0261, JP20257295, and JP21H04434.

Declarations

Conflict of interest The authors declare that they have no conflict of interest.

References

1. Padirac, A., Fujii, T., Rondelez, Y.: Proc. Natl. Acad. Sci. **109**(47), E3212 (2012)
2. Gardner, T.S., Cantor, C.R., Collins, J.J.: Nature **403**(6767), 339 (2000)
3. Elowitz, M.B., Leibler, S.: Nature **403**(6767), 335 (2000)
4. Kim, J., White, K.S., Winfree, E.: Mol. Syst. Biol. **2**(1), 68 (2006)
5. Kim, J., Winfree, E.: Mol. Syst. Biol. **7**(1), 465 (2011)
6. Srinivas, N., Parkin, J., Seelig, G., Winfree, E., Soloveichik, D.: Science **358**(6369) (2017)
7. Montagne, K., Plasson, R., Sakai, Y., Fujii, T., Rondelez, Y.: Mol. Syst. Biol. **7**(1), 466 (2011)
8. Genot, A., Baccouche, A., Sieskind, R., Aubert-Kato, N., Bredeche, N., Bartolo, J., Taly, V., Fujii, T., Rondelez, Y.: Nat. Chem. **8**(8), 760–767 (2016)
9. Weitz, M., Kim, J., Kapsner, K., Winfree, E., Franco, E., Simmel, F.C.: Nat. Chem. **6**(4), 295 (2014)
10. Hasatani, K., Leocmach, M., Genot, A.J., Estévez-Torres, A., Fujii, T., Rondelez, Y.: Chem. Commun. **49**(73), 8090 (2013)
11. Schaffter, S.W., Schulman, R.: Nat. Chem. **11**(9), 829 (2019)
12. Green, L.N., Subramanian, H.K., Mardanlou, V., Kim, J., Hariadi, R.F., Franco, E.: Nat. Chem. **11**(6), 510 (2019)

13. Aufinger, L., Brenner, J., Simmel, F.C.: bioRxiv (2021)
14. Perez-Carrasco, R., Barnes, C.P., Schaerli, Y., Isalan, M., Briscoe, J., Page, K.M.: Cell Syst. **6**(4), 521 (2018)
15. Padirac, A., Fujii, T., Estevez-Torres, A., Rondelez, Y.: J. Am. Chem. Soc. **135**(39), 14586 (2013)
16. Abe, K., Kawamata, I., Shin-ichiro, M.N., Murata, S.: Mol. Syst. Design Eng. **4**(3), 639 (2019)
17. Dehne, H., Reitenbach, A., Bausch, A.: Nat. Commun. **12**(1), 1 (2021)
18. Adleman, L.M.: Science **266**(5187), 1021 (1994)
19. Hagiya, M.: in *International workshop on DNA-based computers* (Springer, 2000), pp. 89–102
20. Genot, A.J., Bath, J., Turberfield, A.J.: J. Am. Chem. Soc. **133**(50), 20080 (2011)
21. Genot, A.J., Bath, J., Turberfield, A.J.: Angew. Chem. Int. Ed. **52**(4), 1189 (2013)
22. Qian, L., Winfree, E., Bruck, J.: Nature **475**(7356), 368 (2011)
23. Qian, L., Winfree, E.: Science **332**(6034), 1196 (2011)
24. Cherry, K.M., Qian, L.: Nature **559**(7714), 370 (2018)
25. Elbaz, J., Lioubashevski, O., Wang, F., Remacle, F., Levine, R.D., Willner, I.: Nat. Nanotechnol. **5**(6), 417 (2010)
26. Xiong, X., Xiao, M., Lai, W., Li, L., Fan, C., Pei, H.: Angew. Chem. Int. Ed. **60**(7), 3397 (2021)
27. Wang, F., Lv, H., Li, Q., Li, J., Zhang, X., Shi, J., Wang, L., Fan, C.: Nat. Commun. **11**(1), 1 (2020)
28. Qu, X., Wang, S., Ge, Z., Wang, J., Yao, G., Li, J., Zuo, X., Shi, J., Song, S., Wang, L., et al.: J. Am. Chem. Soc. **139**(30), 10176 (2017)
29. Takiguchi, S., Kawano, R.: Nanoscale **13**(12), 6192 (2021)
30. Zadorin, A.S., Rondelez, Y., Gines, G., Dilhas, V., Urtel, G., Zambrano, A., Galas, J.C., Estevez-Torres, A.: Nat. Chem. **9**(10), 990 (2017)
31. Aubert-Kato, N., Fosseprez, C., Gines, G., Kawamata, I., Dinh, H., Cazenille, L., Estevez-Torres, A., Hagiya, M., Rondelez, Y., Bredeche, N.: in *Proceedings of the Genetic and Evolutionary Computation Conference* (2017), pp. 59–66
32. Keya, J.J., Suzuki, R., Kabir, A.M.R., Inoue, D., Asanuma, H., Sada, K., Hess, H., Kuzuya, A., Kakugo, A.: Nat. Commun. **9**(1), 1 (2018)
33. Murata, S., Konagaya, A., Kobayashi, S., Saito, H., Hagiya, M.: N. Gener. Comput. **31**(1), 27 (2013)
34. Hagiya, M., Wang, S., Kawamata, I., Murata, S., Isokawa, T., Peper, F., Imai, K.: in *International Conference on Unconventional Computation and Natural Computation* (Springer, 2014), pp. 177–189
35. Hagiya, M., Konagaya, A., Kobayashi, S., Saito, H., Murata, S.: Acc. Chem. Res. **47**(6), 1681 (2014)
36. Douglas, S.M., Bachelet, I., Church, G.M.: Science **335**(6070), 831 (2012)
37. Wickham, S.F., Bath, J., Katsuda, Y., Endo, M., Hidaka, K., Sugiyama, H., Turberfield, A.J.: Nat. Nanotechnol. **7**(3), 169 (2012)
38. Sato, Y., Hiratsuka, Y., Kawamata, I., Murata, S., Nomura, S.i.M.: Sci. Robot. **2**(4) (2017)
39. Wickham, S.F., Endo, M., Katsuda, Y., Hidaka, K., Bath, J., Sugiyama, H., Turberfield, A.J.: Nat. Nanotechnol. **6**(3), 166 (2011)
40. Thubagere, A.J., Li, W., Johnson, R.F., Chen, Z., Doroudi, S., Lee, Y.L., Izatt, G., Wittman, S., Srinivas, N., Woods, D.: et al., Science **357**(6356) (2017)
41. Scalise, D., Schulman, R.: Nat. Comput. **15**(2), 197 (2016)
42. Kishi, J.Y., Schaus, T.E., Gopalkrishnan, N., Xuan, F., Yin, P.: Nat. Chem. **10**(2), 155 (2018)
43. Joesaar, A., Yang, S., Bögels, B., van der Linden, A., Pieters, P., Kumar, B.P., Dalchau, N., Phillips, A., Mann, S., de Greef, T.F.: Nat. Nanotechnol. **14**(4), 369 (2019)
44. Cangialosi, A., Yoon, C., Liu, J., Huang, Q., Guo, J., Nguyen, T.D., Gracias, D.H., Schulman, R.: Science **357**(6356), 1126 (2017)
45. Jaeger, H.: Bonn, Germany: German National Research Center for Information Technology GMD Technical Report **148**(34), 13 (2001)
46. Tanaka, G., Yamane, T., Héroux, J.B., Nakane, R., Kanazawa, N., Takeda, S., Numata, H., Nakano, D., Hirose, A.: Neural Netw. **115**, 100 (2019)
47. Yahiro, W., Aubert-Kato, N., Hagiya, M.: in *Artificial Life Conference Proceedings* (MIT Press, 2018), pp. 31–38
48. Nguyen, H., Banda, P., Stefanovic, D., Teuscher, C.: in *Artificial Life Conference Proceedings* (MIT Press One Rogers Street, Cambridge, MA 02142-1209 USA journals-info@ mit ..., 2020), pp. 491–499
49. Liu, X., Parhi, K.K.: ACS Synthet. Biol. **11**(2), 780–787 (2022)

50. Goudarzi, A., Lakin, M.R., Stefanovic, D.: in *International Workshop on DNA-Based Computers* (Springer, 2013), pp. 76–89
51. Lobato-Dauzier, N., Cazenille, L., Fujii, T., Genot, A., Aubert-Kato, N.: in *Artificial Life Conference Proceedings* (MIT Press, 2020), pp. 420–422
52. Fujii, T., Rondelez, Y.: ACS Nano **7**(1), 27 (2013)
53. Montagne, K., Gines, G., Fujii, T., Rondelez, Y.: Nat. Commun. **7**(1), 1 (2016)
54. Lotka, A.J.: J. Am. Chem. Soc. **42**(8), 1595 (1920)
55. Volterra, V.: Nature **118**(2972), 558 (1926)
56. Tan, E., Erwin, B., Dames, S., Ferguson, T., Buechel, M., Irvine, B., Voelkerding, K., Niemz, A.: Biochemistry **47**(38), 9987 (2008)
57. Rondelez, Y.: Phys. Rev. Lett. **108**(1), 018102 (2012)
58. Jin, Y.: Soft. Comput. **9**(1), 3 (2005)
59. Stiefel, K.M., Ermentrout, G.B.: J. Neurophysiol. **116**(6), 2950 (2016)
60. Zambrano, A., Zadorin, A., Rondelez, Y., Estévez-Torres, A., Galas, J.C.: J. Phys. Chem. B **119**(17), 5349 (2015)